INORGANIC CHEMISTRY FRONTIERS

RESEARCH ARTICLE

View Article Online
View Journal | View Issue

Cite this: *Inorg. Chem. Front.*, 2020, **7**, 2685

Thermal quenching properties of narrow-band blue-emitting $MBe_2(PO_4)_2:Eu^{2+}$ (M = Ca, Sr) phosphors towards backlight display applications

Tao Hu,[a] Yan Gao,[b] Xiaohong Ji,[a] Zhiguo Xia *[a] and Qinyuan Zhang *[a]

Discovering new phosphors with narrow-band emission is critical for white light emitting diodes (LEDs) in liquid-crystal displays (LCDs). Herein, near-ultraviolet (UV) excitable narrow-band blue-emitting $MBe_2(PO_4)_2:Eu^{2+}$ (M = Ca, Sr) phosphors were successfully designed, exhibiting an extremely narrow full width at half-maximum of ~26–27 nm, high color purity of ~99.1%, small Stokes shift of ~1500 cm^{-1}, desirable photoluminescence quantum efficiency of ~63.4%, and zero thermal quenching even at temperatures up to ~300 °C. The small Stokes shift and narrow emission profile are fundamentally caused by the greatly suppressed structural relaxation benefiting from the rigid and ordered connected [BeO_4] and [PO_4] tetrahedra network. Meanwhile, the unprecedented thermal emission behavior is ascribed to the suppression of thermally activated photoionization and the non-radiative pathway from the cross-point of the 5d excited state to the 4f ground state of Eu^{2+}. A wide color gamut reaching up to 88.6% NTSC is realized, demonstrating the validity of $MBe_2(PO_4)_2:Eu^{2+}$ in LED backlights for LCDs. The present studies encourage researchers to identify hitherto undiscovered narrow-band phosphors *via* selecting a stiff and ordered host with confined sites for doped rare earth activators.

Received 22nd April 2020,
Accepted 6th June 2020

DOI: 10.1039/d0qi00467g

rsc.li/frontiers-inorganic

1. Introduction

Phosphor-converted white light emitting diodes (pc-wLEDs) are key components in lighting and display applications for their high efficiency, environmental friendliness and long lifetime.[1–5] Narrow-band emission of a phosphor is critical in the applications of backlighting displays, since it can help to enable wide color gamut to faithfully reproduce natural colors.[6,7] Accordingly, many efforts have been devoted to the discovery of narrow-band phosphors.[8,9] Nevertheless, rare earth Eu^{2+} activated narrow-band phosphors are quite scarce and encounter tremendous challenges in exploration, as evident from there being only a few known narrow-band phosphor families (mainly limited to the UCr_4C_4 family),[10–14] hindering state-of-the-art backlights from further advancing.

The key to an outstanding phosphor lies in the selection of suitable hosts. To identify an efficient phosphor, picking a host with crystal structural rigidity and high atomic connectivity is manifested to be one plausible solution, as suggested previously.[15,16] Beyond that, the band gap (E_g), which plays a decisive role in setting the relative position of the rare earth 5d orbital with respect to the host's conduction band, is related to thermal emission behaviors,[17,18] and thus it is another crucial parameter. Commonly, a sufficiently large E_g in a solid-state compound with rigid crystal structure can prevent an excited 5d electron from photoionizing into the conduction band, and thereby the electron can radiatively return to the 4f ground state rather than photoionize even though at high temperature.[18] To maintain the emission bandwidth at a narrow level, several factors including numbers of potential doping sites, the degrees of structural order/disorder and so on need to be evaluated. Normally a host with multisite occupations as well as chemically different surroundings around the activator could usually lead to a broad spectrum after doping by rare earth activators with 4f–5d transition. Undoubtedly, a crystallographic ordered crystal, in which there is only one cation doping site without statistical occupation is preferential. Therefore, one may deduce, quite literally, that a crystalline ordered, rigid and condensed compound with relatively large E_g and limited doping sites is a suitable narrow-band phosphor candidate.

Initiated by the above mentioned structure–property relationships, alkaline-earth metal beryllophosphates come into view based on several considerations mentioned above. First, phosphates are not only chemically stable but also tend to have a wide E_g (>4 eV),[19,20] signifying their feasibility as

[a]*State Key Laboratory of Luminescent Materials and Devices, Guangdong Provincial Key Laboratory of Fiber Laser Materials and Applied Techniques, School of Materials Science and Engineering, South China University of Technology, Guangzhou, 510641, China. E-mail: xiazg@scut.edu.cn, qyzhang@scut.edu.cn*
[b]*School of Applied Physic and Materials, Wuyi University, Jiangmen 529020, China*

robust hosts with expected thermally stable emission. Second, the crystal structure of beryllophosphate is topologically identical to that of classic hosts of aluminosilicates and borosilicates,[21] which is an indication of beryllophosphates as luminescent hosts. Moreover, the Be–O bond gives rise to a greater degree of covalency compared with Li–O, Mg–O, Al–O and Si–O bonds, making beryllophosphates highly rigid and more likely to achieve fascinating optical properties after doping.[22–25] Third, apparently different from aliovalent substitution cases, in which charge-compensating defects such as vacancies, interstitial ions or ions' valence state change are required, charge compensations are not necessary when Eu^{2+} substitutes for alkaline–earth metal ions because they share the same valence states. As a result, spectral broadening arising from the multitude of charge-compensated Eu^{2+} sites with diverse crystal field splittings can be avoided, and the charge compensating defects killing Eu^{2+} luminescence could be eliminated simultaneously.

To further boost the efficiency LED devices, minimizing the inherent down-conversion energy loss lies in the selection of phosphors with small Stokes shift.[23] Such a small Stokes shift ideally allows shifting the emission of a UV primary pump LED in the blue spectral range, very close to the emission of a blue phosphor. While there is still no commercially available small Stokes shift blue emitting phosphor to the best of our knowledge, the state-of-the-art blue $BaMgAl_{10}O_{17}:Eu^{2+}$ shows efficient emission; however, it is beset by a relatively large Stokes shift and a full width at half-maximum (FWHM) of approximately 55 nm.[26] Making matters worse, it is also not readily excited by 365 or 400 nm light, precluding its use in near-UV LEDs.[27,28] Therefore, the discovery of new near-UV excitable narrow-band blue emitting phosphors is still urgent.

In this work, a kind of brand-new $MBe_2(PO_4)_2:Eu^{2+}$ (M = Ca, Sr) beryllophosphate phosphor was designed and synthesized. Under near-UV excitation, the phosphors exhibit blue emission with high internal quantum efficiency, narrow emission profile, small Stokes shift and zero thermal quenching, addressing the lack of a commercial near-UV pumped narrow band blue phosphor. A prototype pc-wLED utilizing the as-prepared $CaBe_2(PO_4)_2:Eu^{2+}$ (CBPO:Eu^{2+}) yields a wide color gamut, enabling its applications in LCD backlights. Carefully unraveling the structure–property relations for $MBe_2(PO_4)_2:Eu^{2+}$ led us to firmly believe that selecting a structurally ordered and highly rigid host with limited doping sites as well as sizable band gap is the key point to finding an outstanding narrow-band phosphor.

2. Experiments and characteristics

Synthesis

$MBe_2(PO_4)_2:0.02Eu^{2+}$ (M = Ca, Sr) beryllophosphate phosphors were prepared by a conventional solid-state reaction, using $CaCO_3$, $SrCO_3$, BeO, $(NH_4)_2{\cdot}HPO_4$ and Eu_2O_3 as raw materials. The raw materials were in stoichiometric proportions and ground thoroughly. The powder mixtures were placed in aluminum oxide crucibles and sintered at 500 °C for 4 h in air, then reground and sintered at 1050 °C for 4 h under a reducing atmosphere (N_2/H_2 = 95%/5%) in a tube furnace to obtain the products. Note that BeO is of low toxicity. To reduce risk of exposure, the raw materials were weighed and ground thoroughly in a closed glove box.

Characterizations

Powder X-ray diffraction (XRD) measurements were performed with an Aeris X-ray diffractometer (PANalytical Corporation, Netherlands) operating at 40 kV and 15 mA with monochromatized Cu Kα radiation (λ = 1.5406 Å). The electronic band structure calculations were performed in the density functional theory framework, using the Cambridge Serial Total Energy Package (CASTEP) module.[29] The generalized gradient approximations with the Perdew–Burke–Ernzerhof functional were applied to treat the exchange–correlation effects.[30] Ultrasoft pseudopotentials were employed for a description of the interaction between the ionic cores and valence electrons. The photoluminescence, photoluminescence excitation, and temperature-dependent emission spectra were recorded by a Hitachi F-4600 fluorescence spectrophotometer. The quantum efficiency (QE) measurement was performed with a commercial PLQY measurement system of Ocean Optics. The internal QE (η_{int}), defined as the ratio of the number of photons emitted (I_{em}) to the number of photons absorbed (I_{abs}), is expressed as:

$$\eta_{int} = \frac{I_{em}}{I_{abs}} = \frac{\int L_S}{\int E_R - \int E_S} \quad (1)$$

where L_S is the emission spectrum of the sample and E_S and E_R are the spectra of excitation light with and without the sample in the integrating sphere. The luminescence spectrum, luminous efficacy, and correlated color temperature of the constructed w-LED device were measured using an integrating sphere of 1.0 m diameter connected to a CCD detector with an optical fiber.

3. Results and discussion

The XRD patterns of $MBe_2(PO_4)_2:Eu^{2+}$ (M = Ca, Sr) and the standard PDF data of CBPO (PDF#34-1441) and SBPO (PDF#260977) are presented in Fig. 1a and b. Obviously, all the diffraction peaks accord well with their expected Bragg reflection positions, and no additional peaks could be observed, demonstrating the high purity of the two phosphors. The CBPO and SBPO compounds are isostructural with each other, and crystallize in the same monoclinic crystal system and space group $P2_1/c$.[21] Here, we use CBPO as an example to describe the crystal structure. The structure consists of a framework of corner-sharing BeO_4 and PO_4 tetrahedrons assembled in four- and eight-membered rings; these rings are nearly perpendicular to a axis (Fig. 1c). The four-membered rings consist of a pair of tetrahedrons pointing upwards (U) and a pair of tetrahedrons pointing downwards (D), forming

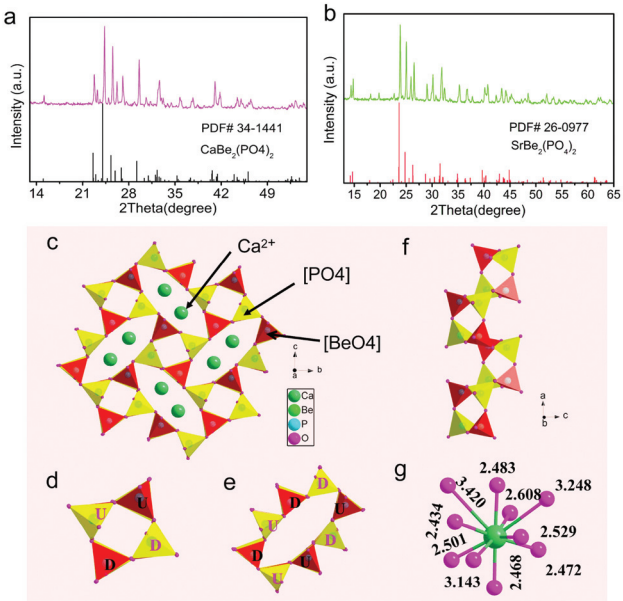

Fig. 1 (a and b) XRD patterns of the $M_2Be_2(PO_4)_2$:Eu^{2+} (M = Ca, Sr) phosphor; Bragg reflection positions of $M_2Be_2(PO_4)_2$ are shown as a reference. The crystal structure of $MBe_2(PO_4)_2$ beryllophosphates: (c) view perpendicular to a axis; (d, e) detailed views of the four- and eight-membered rings with tetrahedra pointed upward (U) and downward (D); (f) detailed view of the double crankshaft chain running parallel to a axis; (g) the local coordination of CaO_{10} polyhedron, showing the bond lengths.

UUDD-type rings (Fig. 1d). While the eight-membered rings are formed by linking four-membered rings, and showing only one pattern of DDUDUUDU (Fig. 1e). The BeO_4 and PO_4 tetrahedrons are also connected by corner-sharing to form a double crankshaft chain running parallel to a axis (Fig. 1f). There is only one crystallographically independent Ca^{2+}/Sr^{2+} site on the Wyckoff position 1*a* in the unit cell of $MBe_2(PO_4)_2$. The Ca^{2+}/Sr^{2+} locate in the eight-membered rings and occur in Ca/SrO_{10} polyhedron (Fig. 1g). Given the similar ionic radius of Eu^{2+} (1.35 Å for ten-fold coordination) and Ca^{2+}/Sr^{2+} (1.23/1.36 Å for ten-fold coordination), the Eu^{2+} activator is expected to substitute for Ca^{2+}/Sr^{2+} ions without introduction of any charge balance defects. In short, the $MBe_2(PO_4)_2$ host is highly connected and condensed with a relatively large degree of condensation of $k \geq 0.5$ (molar ratio of (Be, P):O), as well as only one site for Eu^{2+} to reside, a sign of $MBe_2(PO_4)_2$ having potential for a good phosphor host.

First-principles calculations for the $MBe_2(PO_4)_2$ crystals were performed by the plane-wave pseudopotential method implemented in the CASTEP package. Fig. 2a and c show the calculated distribution curves for the electronic band structures. Obviously, both of them exhibit almost identical band structure profiles, and have a direct semiconductor nature as their maximal energy state in the valence band (VB) and the minimum energy state in the conduction band (CB) both appear at the G point in the Brillouin zone. The energy gaps for CBPO and SBPO are computed as about 5.93 eV and 5.82

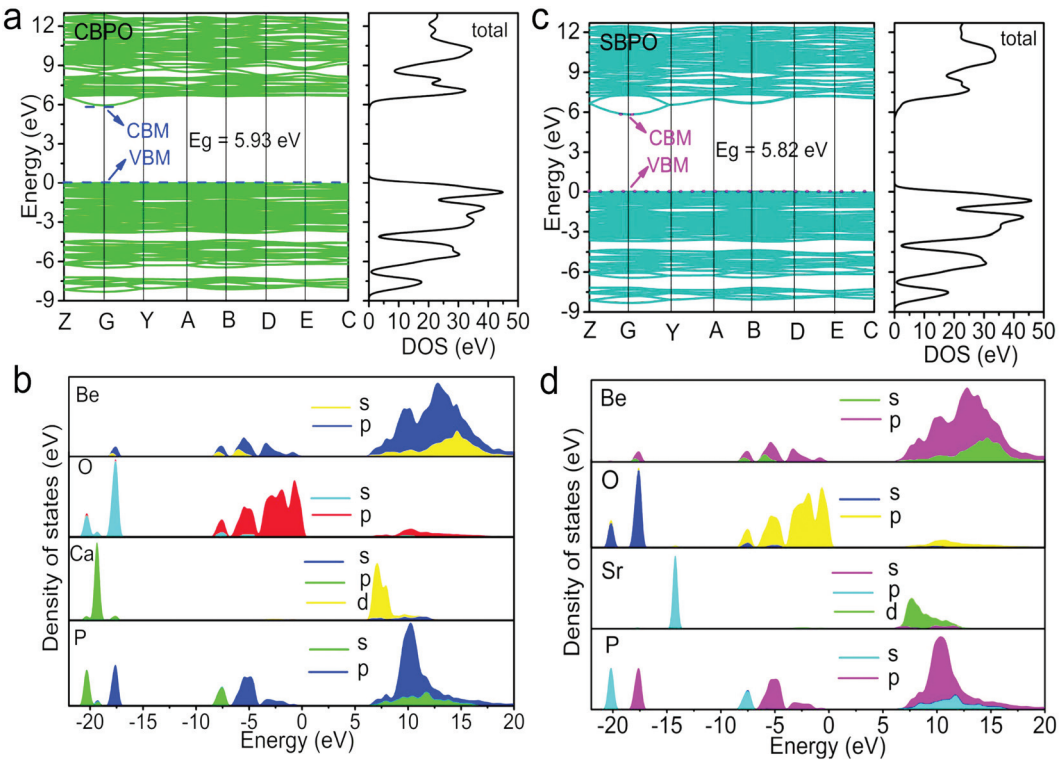

Fig. 2 The calculated energy band structure as well as the total density of states of (a) $Ca_2Be_2(PO_4)_2$ and (c) $Sr_2Be_2(PO_4)_2$ host. The partial (Be, Ca, P, and O atoms) density of states for (b) $Ca_2Be_2(PO_4)_2$ and (d) $Sr_2Be_2(PO_4)_2$.

eV respectively, suitable for resisting against photoionization as discussed below. Compositions of the calculated energy band structures are further resolved by the partial density of states, as shown in Fig. 2b and d. The top of the VB as well as the bottom of CB are found to mainly originate from p orbitals of O^{2-} atoms and d orbitals of Ca^{2+}/Sr^{2+} atoms respectively, with some contributions of p orbitals of Be^{2+} and P^{5+} atoms. Moreover, strong hybridizations of Be^{2+} and O^{2-} orbitals between −8.6 and 0 eV in the VB as well as in the entire CB can be seen, suggesting a strong covalent bonding characteristic of the Be–O bond.

Fig. 3a and b depict the photoluminescence excitation and emission spectra of $MBe_2(PO_4)_2:Eu^{2+}$ phosphor at room temperature. The excitation spectra exhibit a broad band ranging from 200 to 400 nm, and therefore the phosphors can be excited by near-UV light. Under 365 nm UV light excitation, Eu^{2+}-activated CBPO shows blue emission peaking at around 425 nm, while SBPO exhibits violet-blue emission at around 411 nm, ascribed to parity-allowed electric dipole Eu^{2+} $4f^6 5d^1 \rightarrow 4f^7(^8S_{7/2})$ transitions in the EuO_{10} polyhedron. Remarkably, the FWHM of the emission is as narrow as ~26–27 nm, comparable to that of the band-edge exciton emission of typical perovskite semiconductor nanocrystals $CsPbBr_2I_1$ (FWHM = 28.2 nm),[31] and much smaller than that of $BaMgAl_{10}O_{17}:Eu^{2+}$ (FWHM = 50 nm). Such narrow-band emission enables high color purity of ~99.1%, and it is helpful for realizing the wide full-gamut color. The Stokes shift, crudely estimated by doubling the energy difference between maximum emission and the emission/excitation spectra crossing point, is about 1500 cm^{-1}. Of note, the small Stokes shift is typical for weak coupling strength of Eu^{2+} d–f pure electronic transitions with lattice vibrations.

Owing to the 5d electrons being unshielded against the interactions with ligand, the emission profile strongly depends on the lattice. As suggested previously,[27,32] when Eu^{2+} enters into a highly symmetry-coordinated environment such as a cuboid-like polyhedron, the distributions of 5d orbitals are isotropic, beneficial for achieving narrow-band emission. In our case, the Ca/SrO_{10} polyhedrons are highly distorted (characterized by seven short bonds (2.4–2.6 Å) and three long bonds (3.1–3.4 Å)), an indication that the 5d orbitals of Eu^{2+} are anisotropic; specifically the directions of the three long bonds are more delocalized. Based on these facts, we propose that the evenly distributed 5d orbitals might not the primary factor for narrow-band emission, rather it largely relying on local structural rigidity around the Eu^{2+} activator. Thanks to the stiff structure of $MBe_2(PO_4)_2$ arising from the highly rigid connected BeO_4 and PO_4 tetrahedral network, large electronic reconfiguration processes can be enormously suppressed when the Eu^{2+} relaxes from the excited electronic configurational state to the ground state. Therefore, no matter what kind of local structural anisotropies are around Eu^{2+}, a small Stokes shift and narrow band emission can be expected. By contrast, the lack of rigidity, or softness, of a host can lead to a significant reorganization of the excited-state environments and thus to large Stokes shifts and broad FWHM. Moreover, the slightly narrower emission for SBPO:Eu^{2+} (FWHM = 26 nm) compared with CBPO:Eu^{2+} (FWHM = 27 nm) is theoretically

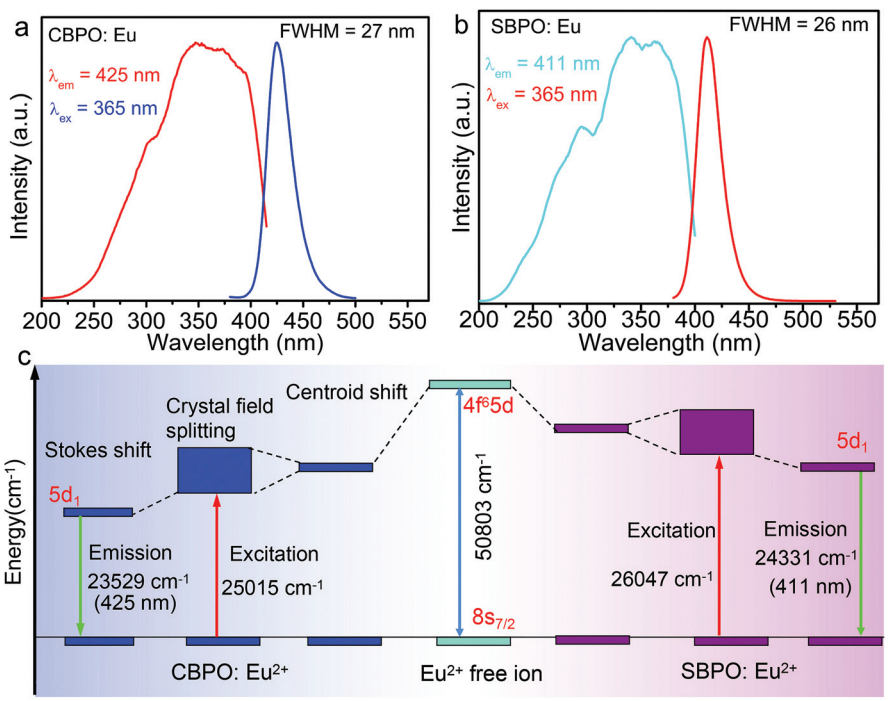

Fig. 3 Room temperature excitation and emission spectra of (a) $Ca_2Be_2(PO_4)_2:Eu^{2+}$ and (b) $Sr_2Be_2(PO_4)_2:Eu^{2+}$ phosphors. (c) Schematic energy level diagram for Eu^{2+} ion in $Ca_2Be_2(PO_4)_2$ and $Sr_2Be_2(PO_4)_2$ crystal structures.

related to the more restricted relaxation for Eu^{2+} on the larger Sr^{2+} site.[33]

The local environment of Eu^{2+} has also a critical effect on d ↔ f transition energies. A larger centroid shift and crystal field splitting generally can lead to a lower energetic transition (Fig. 3c). The centroid shift is positively associated with the covalency of activator–anion bond, also described as nephelauxetic effect, while greater splitting of the 5d level usually comes from a more distorted polyhedron.[34] The Ca/SrO_{10} polyhedrons are characterized using two important parameters, the average bond length l_{av} and the polyhedral distortion index D, to analyze the effects of the centroid shift and the crystal field splitting. The l_{av} for Ca–O is calculated to be 2.72 Å, slightly shorter than that of Sr–O (2.79 Å), reflecting higher covalency and larger crystal splitting energy for CBPO:Eu^{2+}, which shifts the $4f^6 5d$ state to a lower energy in comparison with SBPO:Eu^{2+}. The distortion index D is defined as:

$$D = \frac{1}{n}\sum_{i=1}^{n}\frac{|l_i - l_{av}|}{l_{av}} \quad (2)$$

where l_i is the distance from the center atom to the i^{th} coordinating atom and n is the total number of bonds (n = 10 in this case). The values of D for CBPO and SBPO are then determined to be 0.118 and 0.095, respectively, also demonstrating the larger crystal field splitting, and therefore the red shift of the spectrum for CBPO:Eu^{2+}.

The temperature-dependent emission spectra of $MBe_2(PO_4)_2$:Eu^{2+} in the temperature range of 30–270 °C are depicted in Fig. 4a and d. As temperature increases, emission bands gradually broaden and a slight blue shift is observed, and the mechanism of this variation is discussed below based on previous reports.[35] One important cause is thermally induced lattice expansion, which increases the activator-ligand distance, and thus results in a smaller crystal field splitting and decreasing covalency of the Eu–O bond. Furthermore, thermally induced population of higher vibrational states may lead to a higher emission energy with increasing temperature due to the enhanced electron–phonon strength. The integrated PL intensity as well as emission peak intensity as function of temperature are presented in Fig. 4c and f. The phosphors exhibit extraordinarily stable luminescence against temperature. As can be seen, with increasing temperature, there is almost no significant decrease in peak intensity. Depending on the broadening of spectra with increasing temperature, the intensities at 270 °C for CBPO:Eu^{2+} and SBPO:Eu^{2+} maintain 111% and 127% of that at room temperature, respectively. The zero thermal quenching at high temperature is ascribed to the almost total suppression of thermally activated photoionization and thermally activated cross-over from the 5d excited state to the 4f ground state.[36,37]

Compared with SBPO:Eu^{2+} phosphor that emits violet-blue color, CBPO:Eu^{2+} with narrow-band blue emission and zero thermal quenching is more ideal for near-UV-based LCD backlights. Besides, the non-optimized CBPO:Eu^{2+} also exhibits a favorable internal quantum efficiency of ~63.4%, when excited with 370 nm UV light, further guaranteeing its practical application. Note that beryllium has been disregarded by researchers during the past two centuries because hazardous, fine ber-

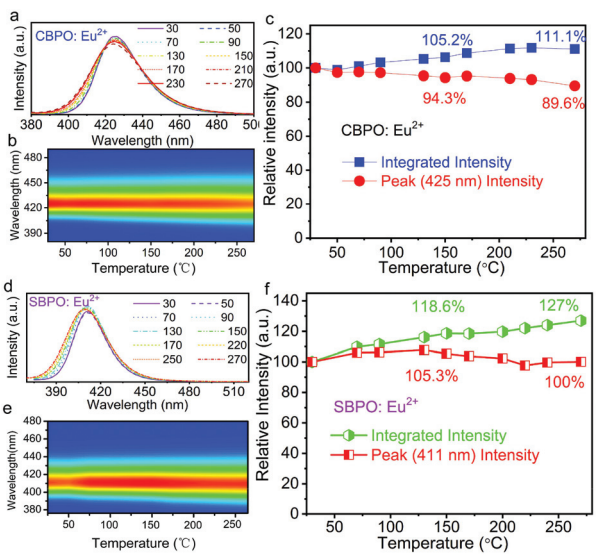

Fig. 4 Temperature-dependent emission spectra of (a and b) $Ca_2Be_2(PO_4)_2$:Eu^{2+} and (d and e) $Sr_2Be_2(PO_4)_2$:Eu^{2+} phosphors in the temperature range of 30–270 °C. Temperature-dependent normalized integrated emission spectra and maximum emission peak intensity of (c) $Ca_2Be_2(PO_4)_2$:Eu^{2+} and (f) $Sr_2Be_2(PO_4)_2$:Eu^{2+} phosphors.

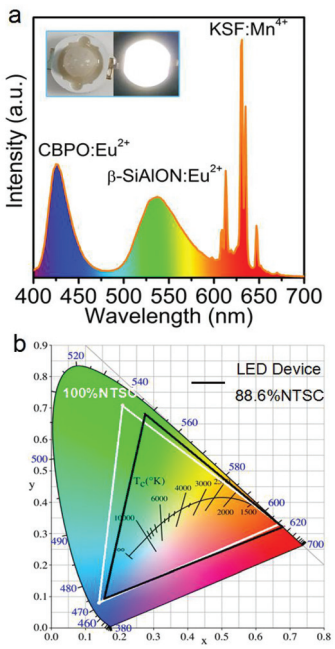

Fig. 5 (a) Emission spectrum of w-LED fabricated by mixing blue $Ca_2Be_2(PO_4)_2$:Eu^{2+}, green β-Sialon:Eu^{2+}, and red K_2SiF_6:Mn^{4+} on a near-UV LED chip (380 nm), under 30 mA driving current. The inset shows photographs of the w-LED device taken under daylight and when it is in operation. (b) Color gamut of the NTSC standard (white triangle) and the as-fabricated w-LED device (black triangle).

yllium dusts can be inhaled and dissolved beryllium salts can accumulate in the human body. In contrast, insoluble and coarsely grained Be-containing solid-state phosphors are less dangerous, especially under appropriate safety measures,[22–25] and therefore, application of CBPO:Eu^{2+} is conceivable. As a proof-of-concept experiment for LCDs, the commercial green β-Sialon:Eu^{2+}, red K_2SiF_6:Mn^{4+} and the as-fabricated blue CBPO:Eu^{2+} were coupled to a commercial 380 nm near-UV chip to construct an LED device. To minimize CBPO:Eu^{2+} blue light being seriously reabsorbed by β-Sialon:Eu^{2+} and K_2SiF_6:Mn^{4+} phosphors, β-Sialon:Eu^{2+} and K_2SiF_6:Mn^{4+} were mixed with binder and coated on the chip first, then CBPO:Eu^{2+} was coated on the surface. Under 30 mA driving current, the constructed prototype w-LED yields bright white light with emission spectrum spanning over the entire visible region (Fig. 5a and inset). Some important photometric and chromaticity parameters of the w-LEDs are listed as: luminous efficiency of 17.6 lm W^{-1}, chromaticity coordinate of (0.306, 0.316), correlated color temperature of 6970 K. The color gamut, defined as the percentage of NTSC in CIE color space, is calculated as 88.6% NTSC. All these results demonstrate that the blue-emitting CBPO:Eu^{2+} phosphor has potential for near-UV-based LCD backlights.

4. Conclusions

In summary, beryllophosphates $MBe_2(PO_4)_2$ (M = Ca, Sr) with highly rigid crystal structure have been studied as previously less regarded phosphor hosts, and have been found to holds potential for achieving optical properties after rare earth activator doping. Only one cation site can be occupied by Eu^{2+} in the $MBe_2(PO_4)_2$ host, and the phosphors present extremely narrow FWHM of ~26–27 nm, a desirable internal quantum efficiency of ~63.4%, as well as zero thermal quenching even at temperatures up to ~300 °C. A w-LED device fabricated by coupling a CBPO:Eu^{2+}/β-Sialon:Eu^{2+}/K_2SiF_6:Mn^{4+} composite with a near-UV-emitting chip yields a color gamut of ~88.6% NTSC, demonstrating CBPO:Eu^{2+} as an efficient blue compensator to improve the color quality and widen the color gamut of w-LED backlights.

Conflicts of interest

The authors declare no conflicts of interest.

Acknowledgements

The present work was supported by the National Natural Science Foundations of China (grant no. 51972118, 51961145101 and 51722202), Fundamental Research Funds for the Central Universities (D2190980), Guangzhou Science & Technology Project (202007020005), the Guangdong Provincial Science & Technology Project (no. 2018A050506004), and the Local Innovative and Research Teams Project of Guangdong Pearl River Talents Program (2017BT01X137).

References

1 P. Pust, P. J. Schmidt and W. Schnick, A revolution in lighting, *Nat. Mater.*, 2015, **14**, 454–458.
2 S. Pimputkar, J. S. Speck, S. P. DenBaars and S. Nakamura, Prospects for LED lighting, *Nat. Photonics*, 2009, **3**, 180–182.
3 E. F. Schubert and J. K. Kim, Solid-state light sources getting smart, *Science*, 2005, **308**, 1274–1278.
4 Z. G. Xia and Q. L. Liu, Progress in Discovery and Structural Design of Color Conversion Phosphors for LEDs, *Prog. Mater. Sci.*, 2016, **84**, 59–117.
5 M. M. Shang, C. X. Li and J. Lin, How to produce white light in a single-phase host?, *Chem. Soc. Rev.*, 2014, **43**, 1372–1386.
6 R.-J. Xie, H. Naoto and T. Takashi, Wide color gamut backlight for liquid crystal displays using three-band phosphor-converted white light-emitting diodes, *Appl. Phys. Express*, 2009, **2**, 022401.
7 H. Lin, T. Hu, Q. M. Huang, Y. Cheng, B. Wang, J. Xu, J. M. Wang and Y. S. Wang, Non-Rare-Earth K_2XF_7: Mn^{4+} (X = Ta, Nb): A Highly-Efficient Narrow-Band Red Phosphor Enabling the Application in Wide-Color-Gamut LCD, *Laser Photonics Rev.*, 2017, **11**, 1700148.
8 T. Hu, H. Lin, Y. Cheng, Q. M. Huang, J. Xu, Y. Gao, J. M. Wang and Y. S. Wang, Highly-distorted Octahedron with C_{2v} Group Symmetry Inducing Ultra-intense Zero Phonon Line in Mn^{4+} Activated Oxyfluoride $Na_2WO_2F_4$, *J. Mater. Chem. C*, 2017, **5**, 10524–10532.
9 M. H. Fang, J. L. Leaño and R. S. Liu, Control of Narrow-Band Emission in Phosphor Materials for Application in Light-Emitting Diodes, *ACS Energy Lett.*, 2018, **3**, 2573–2586.
10 M. Zhao, H. X. Liao, L. X. Ning, Q. Y. Zhang, Q. L. Liu and Z. G. Xia, Next-Generation Narrow-Band Green-Emitting $RbLi(Li_3SiO_4)_2$: Eu^{2+} Phosphor for Backlight Display Application, *Adv. Mater.*, 2018, **30**, 1802489.
11 A. Meijerink, Emerging substance class with narrow-band blue/green-emitting rare earth phosphors for backlight display application, *Sci. China Mater.*, 2018, **62**, 146–148.
12 P. Pust, V. Weiler, C. Hecht, A. Tücks, A. S. Wochnik, A.-K. Henß, D. Wiechert, P. J. Schmidt and W. Schnick, Narrow-band red-emitting $Sr[LiAl_3N_4]$:Eu^{2+} as a next-generation LED-phosphor material, *Nat. Mater.*, 2014, **13**, 891–896.
13 H. X. Liao, M. Zhao, M. S. Molokeev, Q. L. Liu and Z. G. Xia, Learning from a mineral structure toward an ultra-narrow-band blue-emitting silicate phosphor $RbNa_3(Li_3SiO_4)_4$: Eu^{2+}, *Angew. Chem., Int. Ed.*, 2018, **57**, 11728–11731.
14 M. Zhao, H. X. Liao, M. S. Molokeev, Y. Y. Zhou, Q. Y. Zhang, Q. L. Liu and Z. G. Xia, Emerging ultra-narrow-band cyan-emitting phosphor for white LEDs with enhanced color rendition, *Light: Sci. Appl.*, 2019, **8**, 38.

15 K. A. Denault, J. Brgoch, S. D. Kloß, M. W. Gaultois, J. Siewenie, K. Page and R. Seshadri, Average and Local Structure, Debye Temperature, and Structural Rigidity in Some Oxide Compounds Related to Phosphor Hosts, *ACS Appl. Mater. Interfaces*, 2015, **7**, 7264–7272.

16 J. Brgoch, S. P. DenBaars and R. Seshadri, Proxies from Ab Initio Calculations for Screening Efficient Ce^{3+} Phosphor Hosts, *J. Phys. Chem. C*, 2013, **117**, 17955–17959.

17 S. Poncé, Y. Jia, M. Giantomassi, M. Mikami and X. Gonze, Understanding thermal quenching of photoluminescence in oxynitride phosphors from first principles, *J. Phys. Chem. C*, 2016, **120**, 4040–4047.

18 P. Dorenbos, Thermal quenching of Eu^{2+} 5*d*–4*f* luminescence in inorganic compounds, *J. Phys.: Condens. Matter.*, 2005, **17**, 8103–8111.

19 Y. Zhuo, A. Mansouri Tehrani, A. O. Oliynyk, A. C. Duke and J. Brgoch, Identifying an efficient, thermally robust inorganic phosphor host via machine learning, *Nat. Commun.*, 2018, **9**, 4377.

20 J. W. Qiao, L. X. Ning, M. S. Molokeev, Y. C. Chuang, Q. L. Liu and Z. G. Xia, Eu^{2+} site preferences in the mixed cation $K_2BaCa(PO_4)_2$ and thermally stable luminescence, *J. Am. Chem. Soc.*, 2018, **140**, 9730–9736.

21 D. B. Fabrice, H. Frédéric and B. Maxime, Crystal Chemistry of synthetic $M^{2+}Be_2P_2O_8$ (M^{2+} = Ca, Sr, Pb, Ba) beryllophosphates, *Can. Mineral.*, 2014, **52**, 337–350.

22 Y. G. Chen, M. L. Xing, Y. Guo, Z. S. Lin, X. J. Fan and X. M. Zhang, BeO6 Trigonal Prism with Ultralong Be-O Bonds Observed in a Deep Ultraviolet Optical Crystal $Li_{13}BeBe_6B_9O_{27}$, *Inorg. Chem.*, 2019, **58**, 2201–2207.

23 P. Strobel, C. Maak, V. Weiler, P. J. Schmidt and W. Schnick, Ultra-Narrow-Band Blue-Emitting Oxoberyllates $AELi_2[Be_4O_6]$: Eu^{2+} (AE = Sr, Ba) Paving the Way to Efficient RGB pc-LEDs, *Angew. Chem., Int. Ed.*, 2018, **57**, 8739–8743.

24 P. Strobel, R. Niklaus, P. J. Schmidt and W. Schnick, Oxoberyllates $SrBeO_2$ and $Sr_{12}Be_{17}O_{29}$ as Novel Host Materials for Eu^{2+} Luminescence, *Chem. – Eur. J.*, 2018, **24**, 12678–12685.

25 P. Strobel, T. de Boer, V. Weiler, P. J. Schmidt, A. Moewes and W. Schnick, Luminescence of an Oxonitridoberyllate: A Study of Narrow-Band Cyan-Emitting $Sr[Be_6ON_4]$: Eu^{2+}, *Chem. Mater.*, 2018, **30**, 3122–3130.

26 Y. Wang, X. Xu, L. Yin and L. Hao, High thermal stability and photoluminescence of Si-N-codoped $BaMgAl_{10}O_{17}$:Eu^{2+} phosphors, *J. Am. Ceram. Soc.*, 2010, **93**, 1534–1536.

27 A. C. Duke, S. Hariyani and J. Brgoch, $Ba_3Y_2B_6O_{15}$: Ce^{3+}-A high symmetry, narrow-emitting blue phosphor for wide-gamut white lighting, *Chem. Mater.*, 2018, **30**, 2668–2675.

28 B. T. Liu, Y. H. Wang, J. Zhou, F. Zhang and Z. F. Wang, The reduction of Eu^{3+} to Eu^{2+} in $BaMgAl_{10}O_{17}$: Eu and the photoluminescence properties of $BaMgAl_{10}O_{17}$: Eu^{2+} phosphor, *J. Appl. Phys.*, 2009, **106**, 053102.

29 S. J. Clark, M. D. Segall, C. J. Pickard, P. J. Hasnip, M. I. Probert, K. Refson and M. C. Payne, First principles methods using CASTEP, *Z. Kristallogr.*, 2005, **220**, 567–570.

30 J. P. Perdew, K. Burke and M. Ernzerhof, Generalized gradient approximation made simple, *Phys. Rev. Lett.*, 1996, **77**, 3865.

31 W. Zheng, P. Huang, Z. L. Gong, D. T. Tu, J. Xu, Q. L. Zou, R. F. Li, W. W. You, J. C. G. Bünzli and X. Y. Chen, Near-infrared-triggered photon upconversion tuning in all-inorganic cesium lead halide perovskite quantum dots, *Nat. Commun.*, 2018, **9**, 3462.

32 G. J. Hoerder, M. Seibald, D. Baumann, T. Schroder, S. Peschke, P. C. Schmid, T. Tyborski, P. Pust, I. Stoll, M. Bergler, C. Patzig, S. Reissaus, M. Krause, L. Berthold, T. Hoche, D. Johrendt and H. Huppertz, $Sr[Li_2Al_2O_2N_2]$: Eu^{2+}-A High Performance Red Phosphor to Brighten the Future, *Nat. Commun.*, 2019, **10**, 1824.

33 S. Lizzo, A. Meijerink, G. J. Dirksen and G. Blasse, On the luminescence of divalent ytterbium in $KMgF_3$ and $NaMgF_3$, *J. Phys. Chem. Solids*, 1995, **56**, 959.

34 C. Cozzan, G. Laurita, M. W. Gaultois, M. Cohen, A. A. Mikhailovsky, M. Balasubramanian and R. Seshadri, Understanding the links between composition, polyhedral distortion, and luminescence properties in green-emitting β-$Si_{6-z}Al_zO_zN_{8-z}$:Eu^{2+} phosphors, *J. Mater. Chem. C*, 2017, **5**, 10039–10046.

35 T. Wylezich, A. D. Sontakke, V. Castaing, M. Suta, B. Viana, A. Meijerink and N. Kunkel, One ion, many facets: Efficient, structurally and thermally sensitive luminescence of Eu^{2+} in binary and ternary strontium borohydride chlorides, *Chem. Mater.*, 2019, **31**, 8957–8968.

36 J. W. Qiao, Z. Zhao, Q. L. Liu and Z. G. Xia, Recent advances in solid-state LED phosphors with thermally stable luminescence, *J. Rare Earths*, 2019, **37**, 565–572.

37 Y. Wang, J. Ding, Y. Wang, X. Zhou, Y. Cao, B. Ma, J. Li, X. Wang, T. Seto and Z. Zhao, Structural design of new Ce^{3+}/Eu^{2+}-doped or co-doped phosphors with excellent thermal stabilities for WLEDs, *J. Mater. Chem. C*, 2019, **7**, 1792–1820.